JTTEE5 11:233-243

Corrosion Behavior of HVOF-Sprayed and Nd-YAG Laser-Remelted High-Chromium, Nickel-Chromium Coatings

J. Tuominen, P. Vuoristo, T. Mäntylä, S. Ahmaniemi, J. Vihinen, and P.H. Andersson

(Submitted 26 March 2001; in revised form 25 May 2001)

Thermal spray processes are widely used to deposit high-chromium, nickel-chromium coatings to improve high temperature oxidation and corrosion behavior. However, despite the efforts made to improve the present spraying techniques, such as high-velocity oxyfuel (HVOF) and plasma spraying, these coatings may still exhibit certain defects, such as unmelted particles, oxide layers at splat boundaries, porosity, and cracks, which are detrimental to corrosion performance in severe operating conditions. Because of the process temperature, only mechanical bonding is obtained between the coating and substrate. Laser remelting of the sprayed coatings was studied in order to overcome the drawbacks of sprayed structures and to markedly improve the coating properties. The coating material was high-chromium, nickel-chromium alloy, which contains small amounts of molybdenum and boron (53.3% Cr, 42.5% Ni, 2.5% Mo, 0.5% B). The coatings were prepared by HVOF spraying onto mild steel substrates. A high-power, fiber-coupled, continuous-wave Nd:YAG laser equipped with large beam optics was used to remelt the HVOF-sprayed coating using different levels of scanning speed and beam width (10 or 20 mm). Coating that was remelted with the highest traverse speed suffered from cracking because of the rapid solidification inherent to laser processing. However, after the appropriate laser parameters were chosen, nonporous, crack-free coatings with minimal dilution between coating and substrate were produced. Laser remelting resulted in the formation of a dense oxide layer on top of the coatings and full homogenization of the sprayed structure. The coatings as sprayed and after laser remelting were characterized by optical and electron microscopy (OM, SEM, respectively). Dilution between coating and substrate was studied with energy dispersive spectrometry (EDS). The properties of the laser-remelted coatings were directly compared with properties of as-sprayed HVOF coatings.

Keywords corrosion, HVOF, SX-717, laser remelting, Nd-YAG laser

1. Introduction

The high resistance of high-chromium, nickel-chromium alloys to high-temperature oxidation and corrosion makes them widely used as welded and thermally sprayed coatings in fossil fuel-fired boilers, waste incineration boilers, and electric furnaces[1, 2]. Modern thermal spray processes such as high-velocity oxyfuel (HVOF) and plasma spraying are often applied to deposit high-chromium, nickel-chromium coatings onto the outer surface of various parts of boilers, e.g., tubes, to prevent the penetration of hot gases, molten ashes, and liquids to the less noble carbon steel boiler tube. However, the thermal spray coatings exhibit certain drawbacks compared to cast alloy. During thermal spraying the hot particles are exposed to air atmosphere, which results in oxide layers at splat boundaries. In addition, thermal spray coatings may include unmelted particles, residual porosity, and cracks, resulting in an inhomogenous structure, which allows the aggressive corrosive agents (chlorides and sulfates) to reach the substrate and destroy it. The coating layer also can peel off because of a weak mechanical bonding inherent to thermal spray coatings; this is a problem especially at high temperatures and in wet corrosion environments. In contrast, in weld overlays the problem is typically strong Fe dilution from the substrate to the coating, decreasing the coating's corrosion resistance.

Laser surface post-treatment can offer a controlled way of improving the protective properties and bond strength of the sprayed coatings without affecting the substrate properties and dimensions. Laser surface post-treatment of nickel-based alloys

J. Tuominen, P. Vuoristo, T. Mäntylä, and **S. Ahmaniemi,** Tampere University of Technology, Institute of Materials Science, P.O. Box 589, FIN 33101 Tampere, Finland; and **J. Vihinen** and **P.H. Andersson,** Tampere University of Technology, Institute of Production Engineering, P.O. Box 589, FIN 33101 Tampere, Finland. Contact e-mail: jjtuomin@butler.cc.tut.fi.

Table 1 Nominal Composition of SX-717 Spray Powder in wt.%

Powder	Ni	Cr	Mo	B	Si
SX-717	42.5	53.5	2.5	0.5	1.0

Table 2 Diamond Jet Hybrid 2700 HVOF Spraying Parameters

Oxygen (L/min)	150	Powder feed rate (g/min)	60
Propane (L/min)	70	Spray distance (mm)	230
Air (L/min)	360	Surface speed (m/min)	100
Carrier Gas Nitrogen (L/min)	13	Traverse speed (mm/s)	7

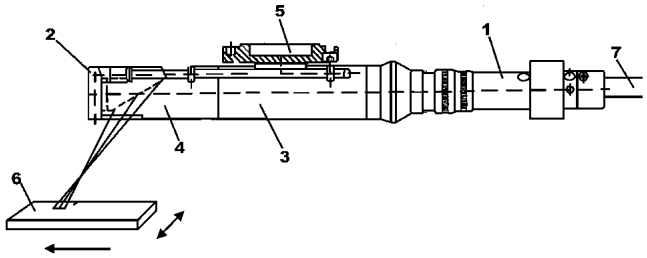

Fig. 1 Experimental setup for laser processing: **(1)** Collimator, **(2)** Integrating mirror, **(3)** Body, **(4)** Mirror head, **(5)** Mounting flange, **(6)** Coating/substrate, **(7)** Optical fiber

Table 3 Nd:YAG Laser Parameters Used in Laser Remelting of HVOF-Sprayed Coating

Power, W	Traverse Speed, mm/min	Beam Width, mm	Specific Energy, Theoretical (J/mm^2)
Mirror 1			
4000	1100	10	21.8
4000	1400	10	17.1
4000	1700	10	14.1
4000	2000	10	12.0
Mirror 2			
4000	400	20	30.0
4000	500	20	24.0
4000	600	20	20.0
4000	700	20	17.1

with low chromium content (<30 wt.%) has been well documented since the late 1970s.[3-5] Few studies have been reported on laser modification of high-chromium, nickel-chromium alloys, perhaps because they are highly sensitive to cracking and exfoliation during the rapid solidification characteristic of laser processing. Moreover, the laser modification used was only superficial laser glazing, where mechanical bonding between coating and substrate remained and alloying of the coating with substrate was neglected.[6,7]

Industrial high-power lasers, CO_2 (up to 45 kW) and Nd:YAG (up to 10 kW) lasers are already well utilized in welding, cutting, and hardening production lines, but not yet in surface engineering, despite the promising results from cladding, alloying, hard phase dispersion, and remelting experiments. High investment costs, low efficiency of the laser source, high maintenance costs, and lack of fundamental knowledge have all discouraged the use of lasers in coating processes. However, because of rapid technological developments of laser devices, especially in direct high-power diode lasers (up to 6 kW), and optics in the last few years, laser surface treatments show very high industrial potential. The lasers are becoming more powerful, enabling faster deposition rates and wider beam widths, which make them interesting also in large surface area applications. The use of optical fibers in Nd:YAG and fiber-coupled diode lasers (previously, fiber coupling for diode lasers was only available up to 2.5 kW), and the development of compact diode lasers offer great opportunities to use industrial robots to treat components and workpieces remote from the laser source. The efficiency of the laser source has been improved significantly, and is 30-50% in high-power diode lasers versus ~15% in CO_2, ~3% in lamp-pumped Nd:YAG, and ~10% in diode-pumped Nd:YAG lasers. Because of shorter wavelength, most of the metals absorb Nd:YAG (1.06 μm) and diode laser (808-940 nm) radiation more efficiently than they absorb CO_2 laser (10.6 μm). High power and efficient beam coupling enable the use of large spot sizes.

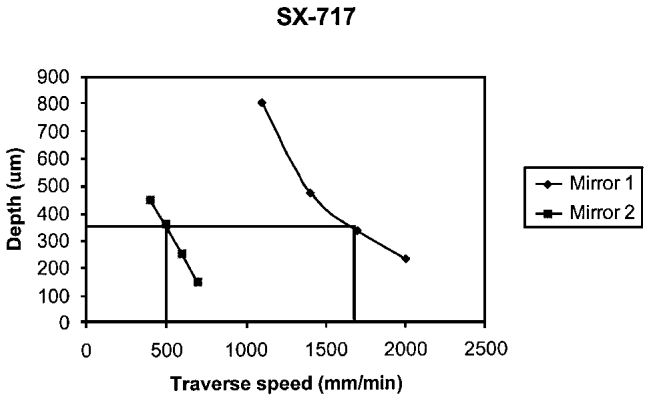

Fig. 2 Melt depth of the laser remelted coatings as a function of traverse speed; original coating thickness is approximately 330-350 μm

This paper investigates wet corrosion properties of the Nd:YAG laser-remelted and HVOF-sprayed high-chromium, nickel-chromium coatings in 3.5 wt.% NaCl. In addition, high-temperature oxidation resistance of the sprayed and remelted coatings at 800°C is studied and compared.

2. Experimental

High-chromium, nickel-chromium coatings were produced using the Diamond Jet Hybrid 2700 HVOF spray system (Sulzer Metco Inc., Westbury, NY). The spray powder was commercial Fukuda SX-717 high-chromium nickel-chromium alloy of particle sizes from 10-45 μm. The composition of powder is shown in Table 1. The propane-fueled Diamond Jet Hybrid 2700 is considered to be a third-generation HVOF process equipped with converging/diverging nozzle, which enhances the velocity of the powder particles, generating very high coating density and a relatively low amount of oxidation. Spraying parameters used are shown in Table 2.

The substrate material was unalloyed low carbon steel Fe 37 with the dimensions of 100 mm × 60 mm × 8 mm. Before the substrates were sprayed, they were degreased in acetone and roughened by alumina (Al_2O_3) grit blasting. The rotating sample holder was used. The thickness of the obtained coatings was approximately 330-350 μm.

The remelting experiments of the sprayed coatings were conducted with a 4 kW, continuous-wave, fiber-coupled HAAS (Haas-Laser GmbH, Schromberg, Germany) HL 4006 D lamp-pumped Nd:YAG laser. The laser light was transported with SiO_2 fiber, 20 m in length and 600 μm in diameter, to hardening optics, which consisted of a collimator and two optional inte-

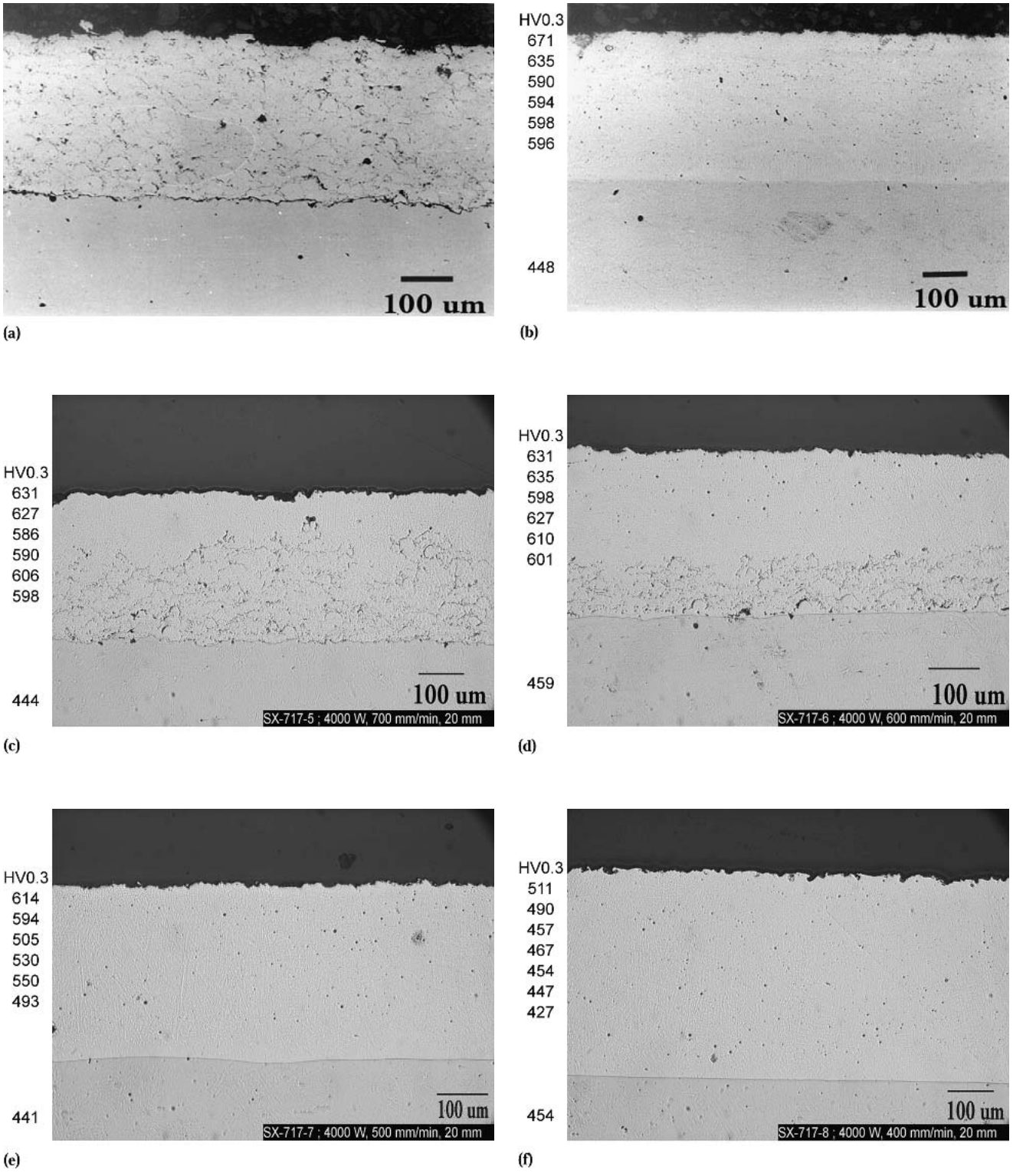

Fig. 3 **(a)** Optical micrograph of HVOF sprayed SX-717 coating; coating thickness is 350 μm. **(b)** Optical micrograph and microhardness values $HV_{0.3}$ of SX-717 coating laser remelted with parameters 4 kW, 1700 mm/min, 10 mm; coating thickness is 350 μm. **(c)** Optical micrograph and microhardness values $HV_{0.3}$ of SX-717 coating laser remelted with parameters 4 kW, 700 mm/min, 20 mm; coating thickness is 350 μm. **(d)** Optical micrograph and microhardness values $HV_{0.3}$ of SX-717 coating laser remelted with parameters 4 kW, 600 mm/min, 20 mm; coating thickness is 350 μm. **(e)** Optical micrograph and microhardness values $HV_{0.3}$ of SX-717 coating laser remelted with parameters 4 kW, 500 mm/min, 20 mm; coating thickness is 350 μm. **(f)** Optical micrograph and microhardness values $HV_{0.3}$ of SX-717 coating laser remelted with parameters 4 kW, 400 mm/min, 20 mm; coating thickness is 450 μm

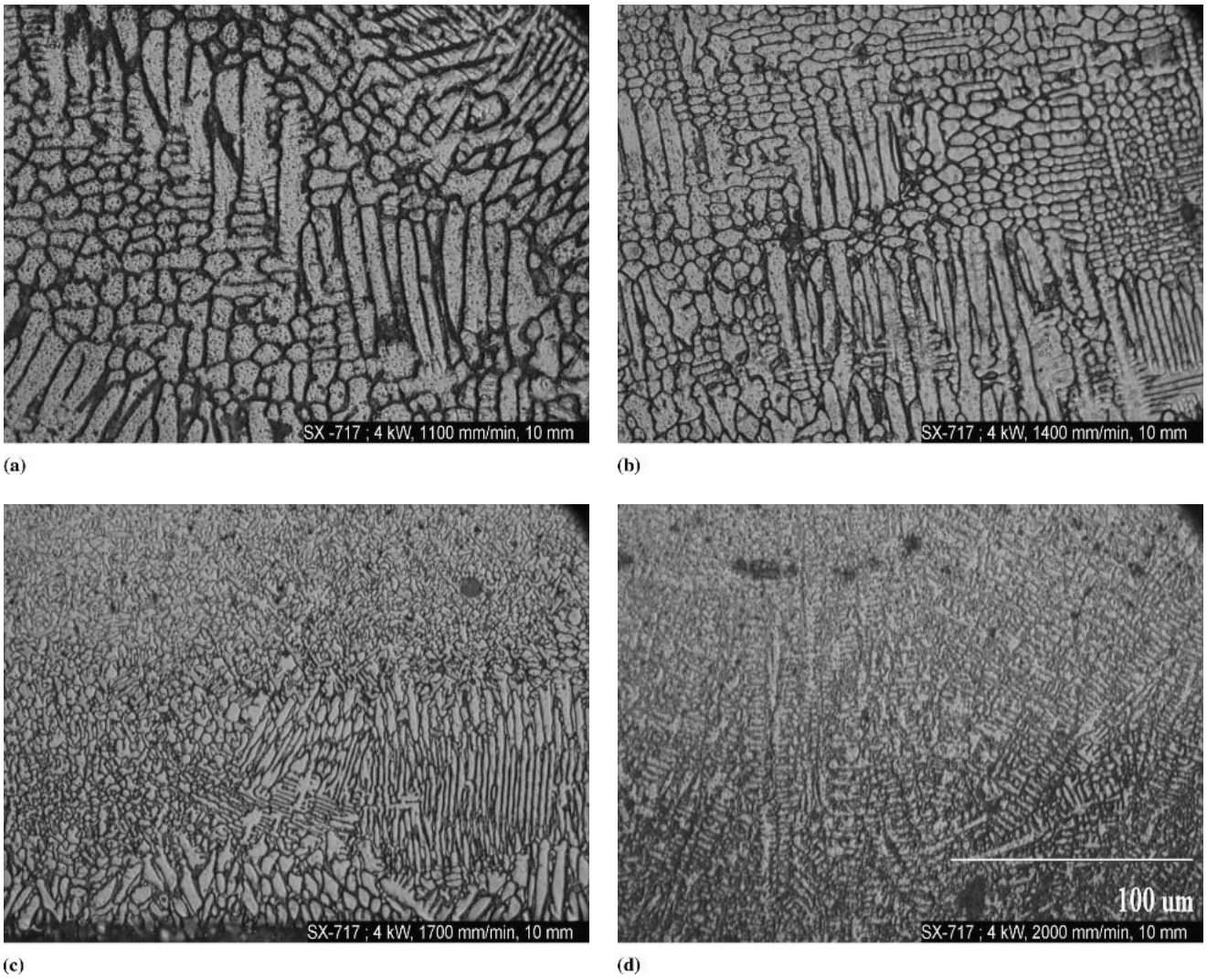

Fig. 4 Optical micrographs of etched SX-717 coating remelted with a power of 4 kW and a traverse speed of **(a)** 1100, **(b)** 1400, **(c)** 1700, and **(d)** 2000 mm/min

grating water-cooled copper mirrors having effective focal lengths of 100 mm. The first mirror (mirror 1) defocuses the rectangular shape of the delivered beam to a spot of size 10 × 8 mm. The second mirror (mirror 2) defocuses the beam to a spot of size 20 × 10 mm, enabling the melt widths of 10 and 20 mm, respectively. Coating samples were mounted on a moving, numerically controlled *x-y* table below the fixed laser processing head. The experimental setup for laser processing of the coating samples is shown in Fig. 1. To remelt the whole surface area of the HVOF-sprayed coating, a series of overlapping passes were made using a constant power of 4 kW, different scanning speeds, and different beam widths (Table 3). Theoretical specific energy (J/mm^2) absorbed by the surface is given by

$$E = P/(bv) \quad \text{(Eq 1)}$$

where P is laser power (W), b is beam width (mm), and v is traverse speed (mm/min). An overlap of 1.5 mm was used with mirror 1, and 1 mm overlap was used with mirror 2. Argon shield gas was blown through the hardening optics onto the workpiece in order to minimize the sample oxidation and to protect the mirror in the processing head.

The coating microstructures were characterized longitudinal and perpendicular to the processing direction by optical microscopy and SEM. To reveal the obtained microstructures, the coatings were etched with a solution of 15 mL HCl (hydrochloric acid), 10 mL CH_3COOH (acetic acid), and 10 ml HNO_3 (nitric acid). The etching time was 40 min.

The SEM instrument used in composition characterization was a Philips (Eindhoven, The Netherlands) XL-30 with an energy-dispersive system (EDS) analyzer.

Microhardness values were measured once on longitudinal cross sections of the coatings starting from the top of the coating and ending at the substrate material. The Vickers method was used with 300 g loads ($HV_{0.3}$ microhardness tester, Shimadzu, Shimadzu Corporation, Kyoto, Japan).

For the immersion tests, the samples were exposed to 3.5 wt.% NaCl solution at room temperature for seven days. During the immersion, the open circuit potential of the coating/substrate system was measured with respect to the Ag/AgCl reference electrode using a high-resistance voltmeter. The area exposed to the electrolyte was 7.6 cm^2, which represented 13% of the whole surface of the sample. The exposed area was restricted by a plastic tube, which was glued to the surface of the sample and filled with the 3.5 wt.% NaCl solution.

Cyclic potentiodynamic polarization measurements were performed in 3.5 wt.% NaCl electrolyte at room temperature using a flat specimen cell (EG&G PARC, Princeton, NJ) in which a 1 cm^2 area of coating surface was exposed to the NaCl solution. The corrosion cell was a glass cylinder horizontally sandwiched between two flat blocks. One block had a circular opening of 11 mm in diameter against which the studied coating surface was pressed. The point of contact between the corrosion cell and coating surface was sealed with a plastic gasket. The potentials were measured with respect to the Ag/AgCl reference electrode, which was connected to the sample through a salt bridge. Measurement started after 5 min of immersion in the electrolyte. A platinum electrode was used as a counter electrode. The scanning speed was 0.5 mV/s.

High-temperature oxidation tests were carried out in a tube furnace at 800°C in air atmosphere for 100 h. The oxidized coating samples were then mounted in epoxy for microstructural studies and for the thickness measurements of the formed oxide layer.

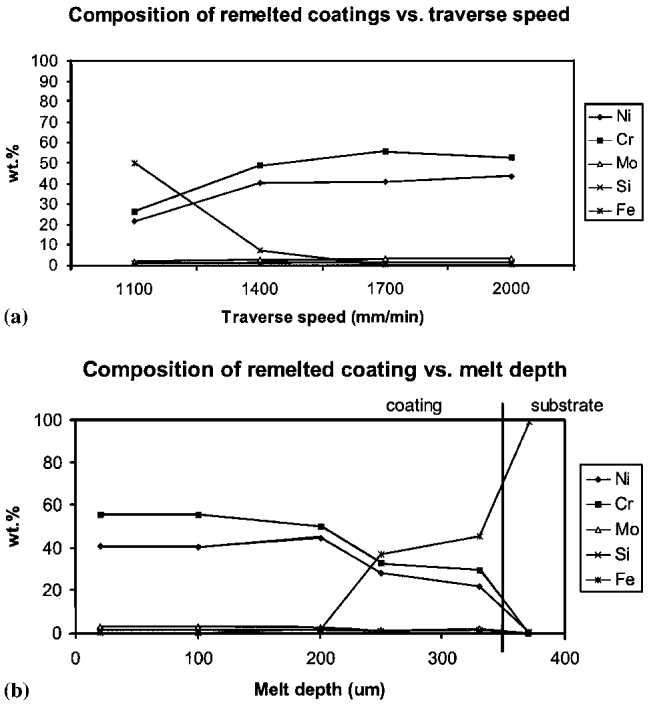

Fig. 5 **(a)** Composition of remelted SX-717 coatings versus traverse speed at a depth of 20 μm. **(b)** Composition of SX-717 coating remelted with parameters 4 kW, 1700 mm/min, 10 mm versus melt depth

3. Results and Discussion

The laser parameters used with mirror 1 were optimized to fully melt the HVOF-sprayed coating except in one set of parameters (4 kW and 2000 mm/min), which melted the coating only partly to the depth of 200-250 μm, leaving the sprayed structure beneath the melted layer and causing mechanical bonding between coating and substrate. The melt depths of the other samples increased from 330-800 μm when the specific energy absorbed by the surface was increased by slowing down the traverse speed from 1700-1100 mm/min (Fig. 2). When the original thickness of the sprayed coating was measured to be approximately 330-350 μm before laser treatment, the samples treated with parameters 4 kW and 1700 mm/min showed the melt depth close to the original thickness of the coating. Laser parameters with slower traverse speed, i.e., higher specific energy, produced melt deeper than 350 μm, indicating high dilution and mixing between the coating and substrate. It was also noted that obtained surface morphology was strongly influenced by traverse speed. With low traverse speed the melt pool solidified to the shape, where material was clustered from both sides of the track to the center of the track, generating an irregular surface. According to Mahank et al.,[8] this happens because surface tension forces are present in the melt pool. Samples treated with slow traverse speed also exhibited strong slag formation within the 1.5 mm area where the adjacent beams were overlapped.

The melt depths achieved with mirror 2 were more ambiguous. The melt depth of a single track is always deeper in the side of the track, where the laser beam enters more perpendicularly to the surface, as shown in Fig. 1. In the other side of the track, the laser beam enters less perpendicular to the surface and is therefore reflected strongly from the coating surface. Hence, the power density of the laser beam was not as homogeneous after mirror 2 than after mirror 1. Thus, for mirror 2 the melt depths were measured from the center of the track, which is an average melt depth of a single track (Fig. 2). It can be noted that parameters set 4 kW, 400 mm/min and 4 kW, 500 mm/min enabled the sprayed coatings to melt fully. A traverse speed of 500 mm/min showed the melt depth close to the original thickness of the coating. It is markedly lower than 1700 mm/min, which produced the same melt depths in remelting with mirror 1. Increasing beam spot decreases the specific energy absorbed by the surface, which explains the difference in traverse speeds between mirrors 1 and 2.

The microstructures of the as-sprayed and laser-remelted coatings are shown in Fig. 3(a-f). The layered microstructure in HVOF-sprayed coating is clearly seen. Layers of oxides at intersplat boundaries as seen in Fig. 3(a) are typical for metallic alloys. During spraying, molten powder particles are exposed to air and are oxidized in flight to the substrate. Oxidation can also occur at the exposed surface of splats prior to the deposition of the subsequent layer.[9] Mechanical bonding between the coating and substrate as well as some pores can be seen. Microhardness values measured from the sprayed coating varied between 351 and 533 $HV_{0.3}$ because of the difference in the indentation sites (pores and oxides). A relatively wide microhardness value range is typical for an inhomogeneous sprayed structure. Microhardness of the substrate is 180 $HV_{0.3}$.

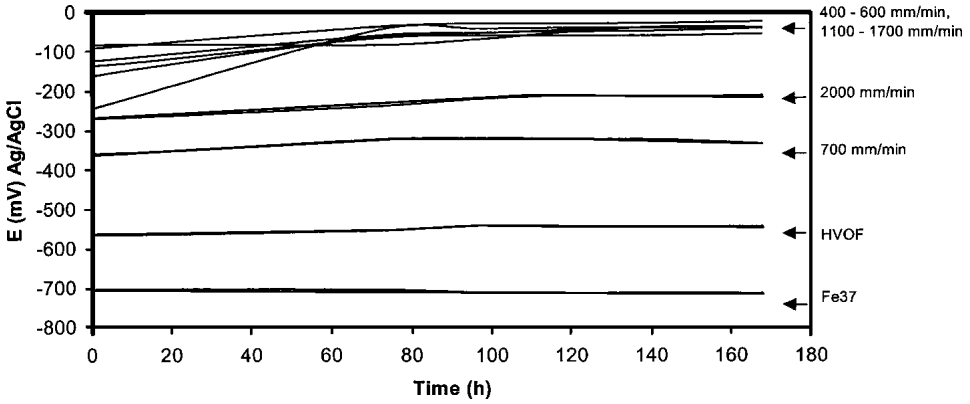

Fig. 6 Open circuit potential versus time measured in 3.5 wt.% NaCl solution for laser-remelted and HVOF-sprayed SX-717 coatings

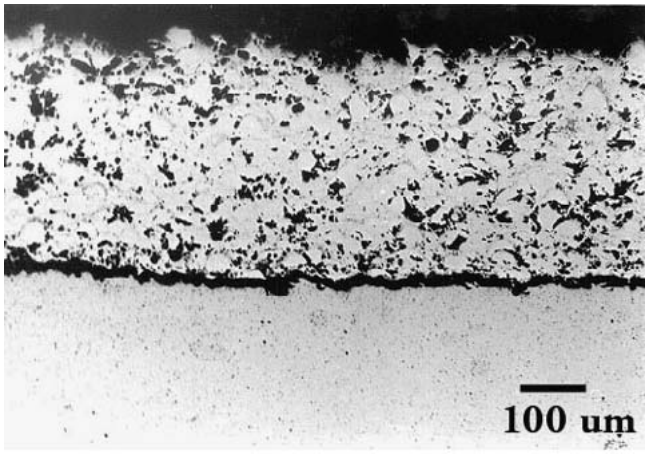

(a)

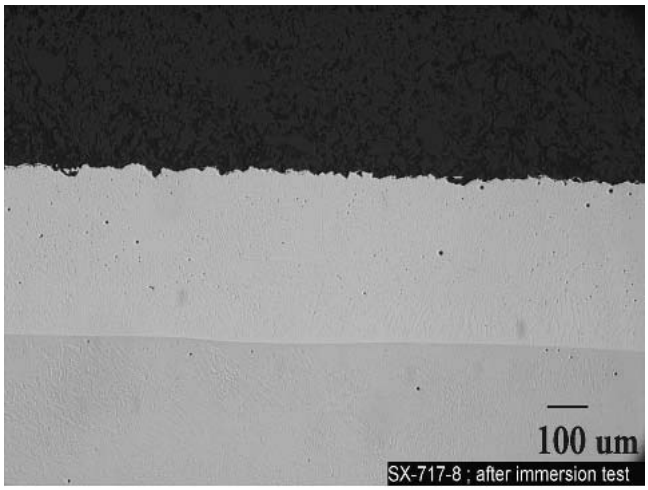

(b)

Fig. 7 **(a)** Optical micrograph of a HVOF sprayed SX-717 coating after a 1 week immersion test in 3.5 wt.% NaCl solution. The electrolyte has corroded the substrate and the coating selectively; coating thickness is 350 μm. **(b)** Optical micrograph of laser remelted SX-717 coating after a 1 week immersion test in 3.5 wt.% NaCl solution. The coating seems to be unaffected; coating thickness is 450 μm.

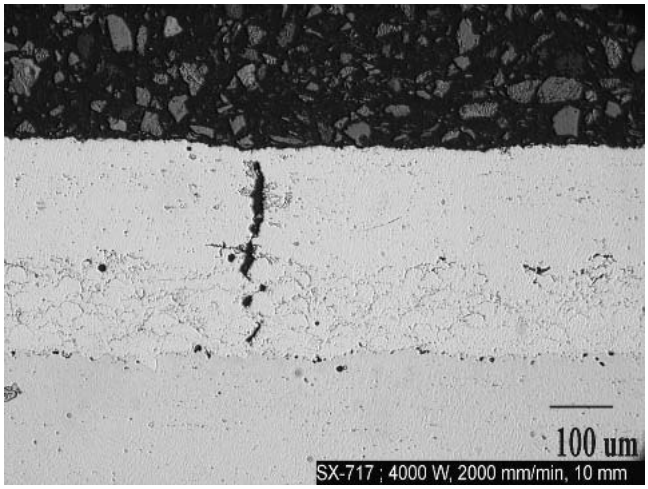

Fig. 8 Optical micrograph of SX-717 coating remelted with parameters 4 kW, 2000 mm/min, 10 mm. A vertical crack is clearly seen.

The coatings obtained using laser remelting were metallurgically dense, and free of cracks and pores, as seen in Fig. 3(b-f). Some vertical cracks were, however, detected from the sample processed with mirror 1 and with parameters 4 kW, 2000 mm/min. The solidification rate of coating material increased, when the traverse speed was increased. The sample, which included vertical cracks, was processed with the highest traverse speed of this experiment. Metallurgical bonding was obtained between coating and substrates, when the specific energy absorbed by the surface was high enough. Microhardness values of the remelted coatings were markedly higher than those of the sprayed coating. Coatings remelted with mirror 2 showed a clear increasing tendency toward microhardness, when the traverse speed was increased from 400-700 mm/min. The highest microhardness values were measured on the sample that was remelted with mirror 1 and with parameters 4 kW, 1700 mm/min. Microhardness of the substrate increased to values of 440-450 $HV_{0.3}$.

Obtained microhardness values of the remelted coatings can be explained by Fe dilution from the substrate to coating and

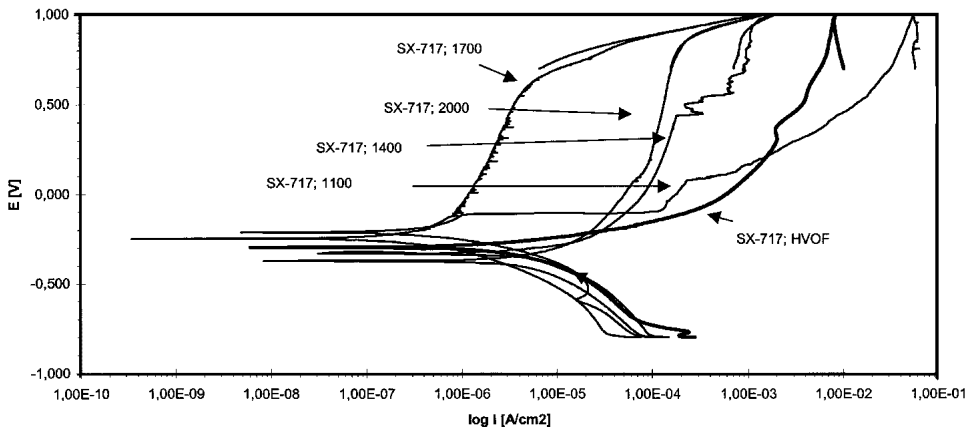

Fig. 9 Cyclic polarization curves of remelted (mirror 1) and HVOF-sprayed SX-717 coatings

solidification rates. From the figures of the etched microstructures, it can be seen that higher traverse speed generates finer microstructure because of the higher solidification rate (Fig. 4a-d). The role of diluted Fe in the grain size of the microstructure has not yet been studied. The amount of Fe decreases from the 50.0 wt.% to below the detection limit when the traverse speed was increased from 1100-2000 mm/min measured at a depth of 20 μm from the top of the coating (Fig. 5a). In a sample remelted with parameters 4 kW, 1700 mm/min, for which the melt depth was very close to the original thickness of the coating, iron concentration was still undetectable at a depth of 100 μm and only 1.5 wt.% at a depth of 200 μm, from where it begins to increase to 36.8 wt.% at a depth of 250 μm (Fig. 5b).

3.1 Immersion Test/Open Circuit Potential (OCP)

For the HVOF-sprayed coating, the open circuit potential value versus Ag/AgCl reference electrode started to move to the more negative direction immediately after exposure to the 3.5 wt.% NaCl solution, indicating active corrosion behavior (Fig. 6). At the same time, it was noted that after a couple of hours from the beginning of the test, the first corrosion products appeared more or less evenly on the whole surface of the exposed coating. Because of the interconnected pores, splat boundaries, and microcracks characteristic of sprayed coatings, the electrolyte quickly reached the substrate and corroded it, as shown in Fig. 7(a). The coating material itself also was corroded strongly. It seems that the deterioration of the coating was initiated along splat boundaries and corroded the material nearby. In our previous studies, similar degradation was found at splat boundaries in HVOF-sprayed IN-625 (Ni-Cr-Mo) coating exposed to 3.5 wt.% NaCl solution. Similarly, Dent et. al.[9] noticed the same kind of degradation in HVOF-sprayed Ni-Cr-Mo-B coating exposed to 0.5 M H_2SO_4, especially when significant oxidation had occurred during spraying. According to Edris et al.,[10] HVOF-sprayed NiCrMo coating includes a certain amount of low alloy Ni-based regions, which suffer from chromium depletion. The existence of these regions depends on the amount of oxide (Cr_2O_3, $NiCr_2O_4$) layers at splat boundaries. After 1 h from the beginning of the test, the open circuit potential value stabilized to the level of −540 mV, which is approximately 200 mV higher than the potential measured from the uncoated Fe 37, indicating the more noble character of the sprayed coating than that of the substrate. When electrolyte connection was established between the coating and substrate, a galvanic pair was generated, and the substrate was acting as an anode and the coating was acting as a cathode. In this case the coating was cathodically protected and the substrate corroded quickly because of the electrolyte connection and high surface area ratio.

Laser-remelted coatings showed another kind of behavior. For coatings remelted with traverse speeds 1100-1700 mm/min (mirror 1) and 400-600 mm/min (mirror 2), the open circuit potential started to change to a more positive direction after exposure to electrolyte, indicating passivation of the coating material. After 1 week of immersion, the surface of the exposed areas was still free of any corrosion products and microstructure was unaffected, as shown in Fig. 7(b). Open circuit potential was noted to be 700 mV more positive than that of uncoated Fe 37 and 500 mV more positive than that of HVOF-sprayed coating. Coating remelted with the highest traverse speed, 2000 mm/min (mirror 1), allowed the electrolyte to pass the coating through vertical cracks shown in Fig. 8, which were formed as a result of too rapid solidification. Open circuit potential stabilized to the level of −200 mV. Coating remelted with the traverse speed of 700 mm/min (mirror 2) allowed the electrolyte to reach the substrate from near the area where two adjacent beams overlapped. The specific energy absorbed by the surface was not high enough to melt the side of the track, where the laser beam entered less perpendicularly.

The open circuit potential measurement of the coating/substrate system is, as shown in the above results, a rather simple method to reveal connection between electrolyte and substrate. The curves of the best laser-remelted coatings did not show any effect of the substrate because the coating totally separated the electrolyte from the substrate, whereas the curve of HVOF-sprayed coating was strongly dominated by the substrate behavior because of the interconnected paths.

The reasons the cracks allow the electrolyte to pass the coating and to corrode the substrate is a shrinkage stress and the relatively hard and brittle nature of coating material. For high-chromium, nickel-chromium alloy, the coefficient of thermal expansion (11.7×10^{-6}/°C for SX-717) is very close to that of the substrate Fe 37 (11.7×10^{-6}/°C for pure Fe, 12.0×10^{-6}/°C for 0.25% C steel).[11] Despite the relatively similar coefficients of thermal expansion, vertical cracking occurred. During laser remelting the transient and nonuniform temperature fields are usually formed. They cause different zones of the material to expand by different amounts. In addition, the coefficient of thermal expansion in metals increases at elevated temperatures (52 wt.% Ni-48 wt.% Cr; 11.8×10^{-6}/°C from 26-93°C, 12.8×10^{-6}/°C from 26-260°C, 13.8×10^{-6}/°C from 26-538°C, 15.0×10^{-6}/°C from 26-816°C, and 15.4×10^{-6}/°C from 26-1038°C).[12] Consequently, the hotter surface of the remelted coating expanded more in rapid heating and shrunk more in rapid cooling compared to the cooler part of the sprayed coating beneath the remelted zone. Shrinkage stress due to temperature difference and mismatch of the coefficients of thermal expansion between the top of the coating and the area close to the coating/substrate interface exceeded the tensile strength of the coating material and cracking occurred. SX-717 alloy as a sprayed coating resists cracking and delamination during heating cycles better than traditional high-chromium, nickel-chromium alloys, which have significantly smaller coefficient of thermal expansion (e.g., 7.5×10^{-6}/°C for Ni-45%Cr). In laser remelting, however, relatively high traverse speed (2000 mm/min) caused a sharp thermal gradient, which influenced the thermal expansion behavior of coating material, resulting in the formation of cracks.

Crack formation can be reduced by preheating the coating/substrate system before melting. As the temperature difference between coating and substrate (i.e., the high thermal gradient produced by intensive laser beam) is reduced, the probability of crack formation is smaller. Another method to decrease the solidification rate and to decrease the number of cracks is to decrease the traverse speed, but at the same time laser power must be decreased as well in order to avoid excess dilution between coating and substrate. To this end the use of a wider beam is beneficial. It results in lowering of the solidification rate while maintaining the high laser power by decreasing only the traverse speed without slowing markedly the process speed, because the area treated by one laser pass is twice as large.

3.2 Electrochemical Measurements

Figure 9 shows the cyclic polarization curves for the HVOF-sprayed and laser-remelted coatings with mirror 1 measured in 3.5 wt.% NaCl solution. The coating remelted with slowest traverse speed and the sprayed coating exhibited the poorest corrosion resistance in the solution showing the highest current densities, the narrowest passivation area, and the positive hysteresis loops. HVOF-sprayed coating showed not a rapid, but a steady increase in current density, and a small passivation area between +300 and +350 mV. During cyclic polarization measurement, the HVOF-sprayed coating suffered from substrate/coating interface corrosion because of interconnected paths, which could have been microcracks or pores, but most likely were splat boundaries. It suffered also from crevice corrosion on top of the

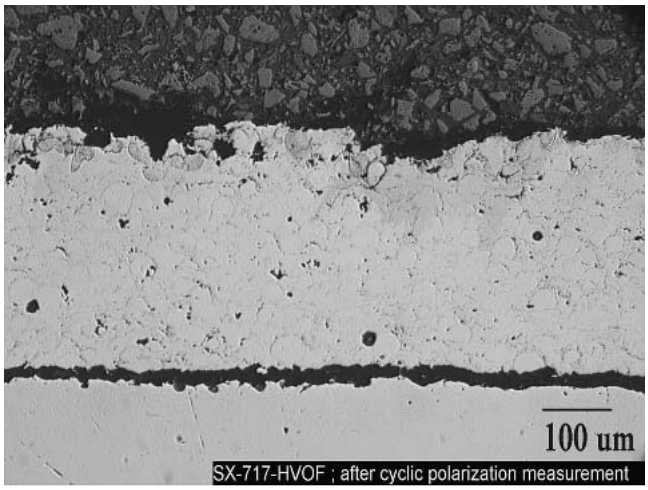

(a)

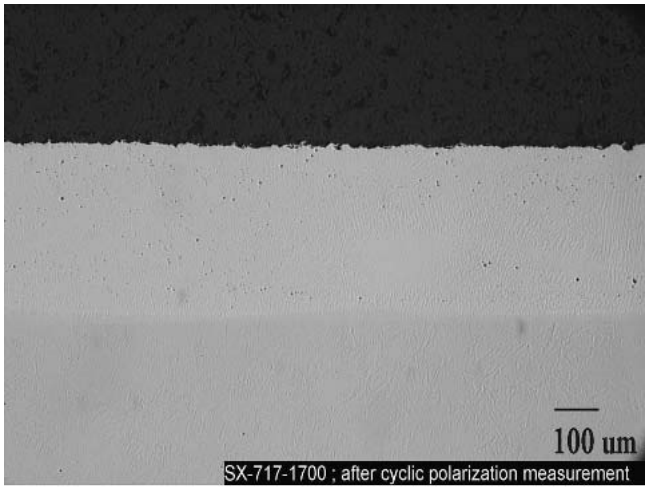

(b)

Fig. 10 **(a)** Optical micrograph of HVOF-sprayed SX-717 coating after cyclic polarization measurement; coating thickness is 350 μm. **(b)** Optical micrograph of SX-717 coating remelted with parameters 4 kW, 1700 mm/min, 10 mm after cyclic polarization measurement; coating thickness is 350 μm

coating because of a weak oxide layer or localized imperfections in the passive layer, as shown in Fig. 10(a). The coating remelted with the slowest traverse speed shows very rapid increase in current density already at −104 mV, which illustrates the breakdown of passivity in the passive oxide layer, indicating strong pitting or crevice corrosion. A positive hysteresis loop is also formed as the direction of scan is reversed, owing to continued and accelerated corrosion in the pits. Strong crevice formation was detected visually from the surface of tested coating, especially from the areas that were under the plastic gasket during the measurement. Strong iron dissolution from the substrate had changed the composition of the coating, thus weakening the protective oxide layer on top of the coating. Coatings remelted with higher traverse speeds showed markedly lower current densities in the passive region, wider passivation areas, and negative hysteresis loops. In the coatings, for which dilution has been limited (4 kW, 1700 mm/min) or zero (4 kW, 2000 mm/min), no break-

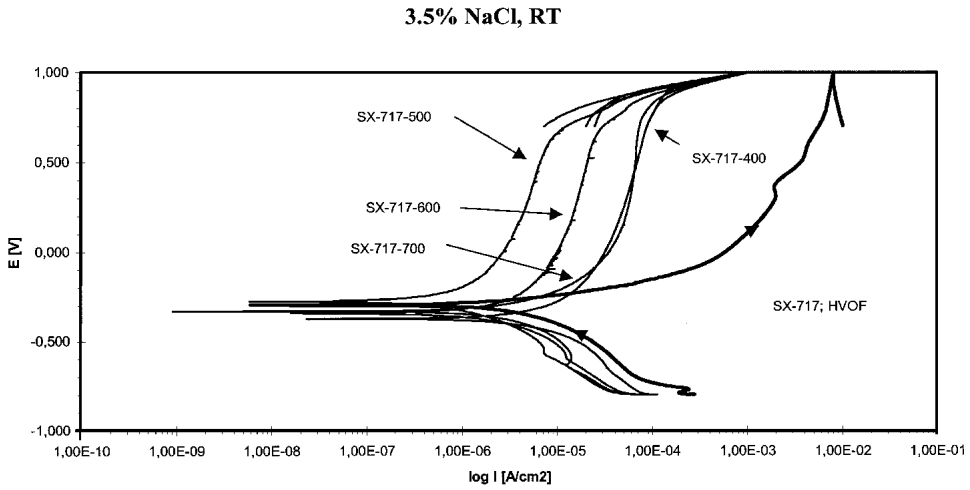

Fig. 11 Cyclic polarization curves of remelted (mirror 2) and HVOF-sprayed SX-717 coatings

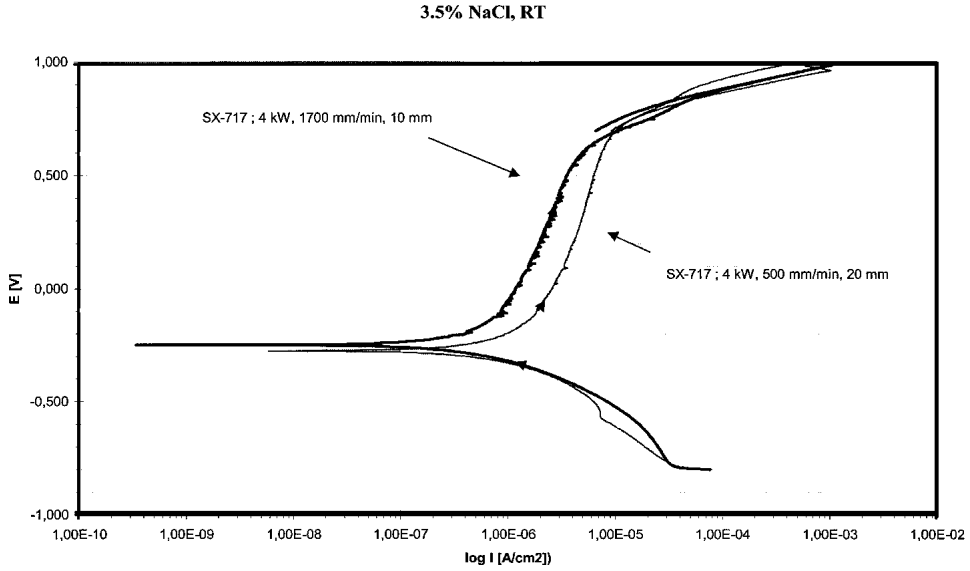

Fig. 12 Cyclic polarization curves of the SX-717 coatings remelted with mirror 1 and mirror 2 and different traverse speeds

down potential could be seen, indicating excellent resistance to localized corrosion resulting from a strong and dense oxide layer. The unaffected microstructure of the laser-remelted coating after cyclic polarization measurement is seen in Fig. 10(b). Coating remelted with parameters 4 kW, 1400 mm/min shows breakdown potential at +450 mV; slight crevice formation was also detected from the surface of the coating.

Figure 11 shows the polarization curves for the coatings laser remelted with mirror 2. All of these coatings show markedly lower current densities, wider passivation areas, and negative hysteresis loops compared with sprayed coating. Because of parameters used with mirror 2, the dilution between coating and substrate was very controlled, explaining the results from the polarization measurements. All of these coatings seemed to be unaffected without any signs of corrosion pits or crevices. Again, the best corrosion behavior was exhibited by the sample that was melted to the depth of the original sprayed coating thickness, and the poorest corrosion behavior was exhibited by the coating remelted with the slowest traverse speed.

If we compare the best curves from the remelting series with mirror 1 and 2, the parameters 4 kW, 1700 mm/min show slightly lower current densities than 4 kW, 500 mm/min (Fig. 12). Markedly higher traverse speed (1700 versus 500 mm/min) generates finer microstructure, which perhaps causes the slight difference in current densities in favor of coating remelted with traverse speed 1700 mm/min.

3.3 High-Temperature (HT) Oxidation Test

Microstructures of the tested samples revealed that HVOF-sprayed coating suffered from oxidation, whereas laser-remelted coatings did not. The latter did not reveal any deterio-

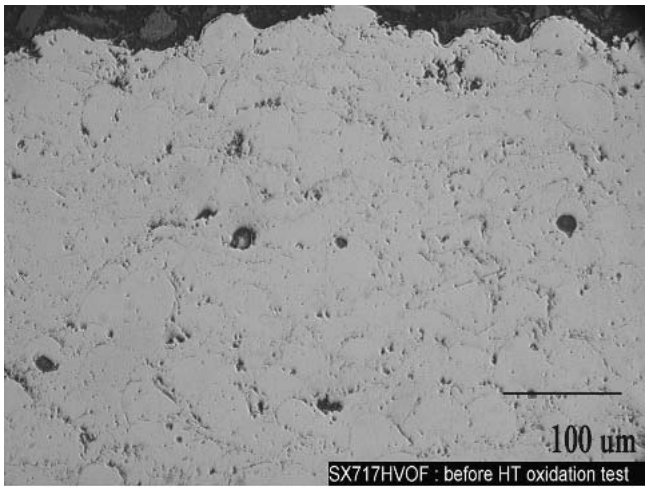

(a)

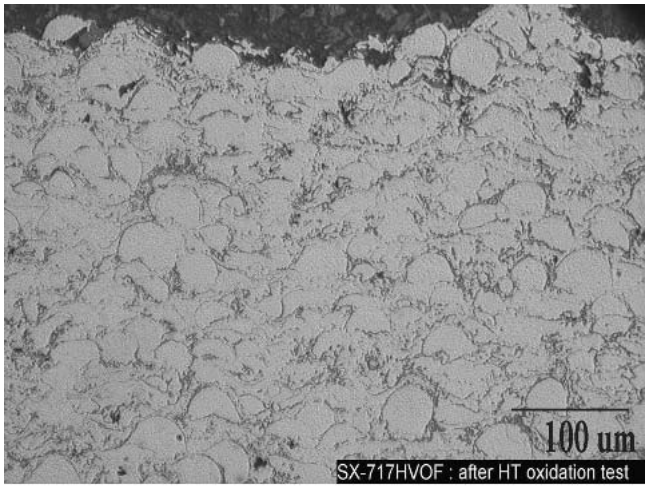

(b)

Fig. 13 **(a)** Optical micrograph of HVOF-sprayed SX-717 coating before HT oxidation test; **(b)** optical micrograph of HVOF-sprayed SX-717 coating after HT oxidation test

ration, indicating excellent HT oxidation resistance because of a very thin and dense oxide layer on top of the coating. Microstructures of the sprayed coating before and after the HT oxidation test showed clearly that the amount of oxidation along splat boundaries had increased (Fig. 13). It can be concluded that the oxide layer formed on top of the sprayed coating was not dense enough to prevent the propagation of oxygen to the coating structure. The unaffected microstructure of the laser-remelted coating after the HT oxidation test is shown in Fig. 14.

4. Conclusions

The experiments performed in this study showed that the general and localized corrosion resistance of the HVOF-sprayed, high-chromium, nickel-chromium coating in an aqueous chloride solution can be improved significantly by using laser surface remelting with appropriate processing parameters.

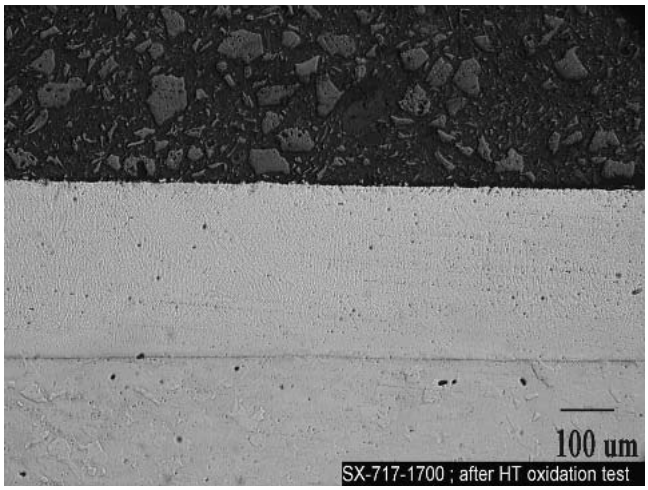

Fig. 14 Optical micrograph of laser remelted (4 kW, 1700 mm/min) coating after HT oxidation test; coating thickness is 330 μm

The laser parameters generating too high specific energy should be avoided, because iron dilution from the substrate to coating decreases the pitting corrosion resistance and microhardness of the coating. Because the high-chromium, nickel-chromium alloy is highly sensitive to cracking, the high solidification rates should be avoided by using lower traverse speed in remelting. The traverse speed can be decreased by using a wider beam (20 mm instead of 10 mm) without lowering markedly the productivity of the surface treatment. This speed results in the elimination of cracks in laser-remelted coatings.

Laser remelting improved markedly the HT oxidation resistance of the HVOF-sprayed coating. Laser remelting resulted in the formation of a very thin and dense oxide layer on top of the coating, giving excellent resistance to oxidation at 800°C in atmosphere.

Acknowledgments

The authors are grateful to the National Technology Agency TEKES, Valmet Corp., Ahlstrom Machinery Corp., and Imatra Steel Oy Ab for financial support of the present work. We would also like to thank Mr. Mikko Kylmälahti for technical support and HVOF spraying of the samples.

References

1. Y. Kawahara: "Development and Application of High Temperature Corrosion-Resistant Materials and Coatings for Advanced Waste-to-Energy Plants," *Mater. High Temp.,* 1997, *14*(3), pp. 261-68.
2. E.J. Morgan-Warren: "Thermal Spraying for Boiler Tube Protection," *Welding Met. Fabric.,* 1992, *January/February,* pp. 25-31.
3. G.C. Irons: "Laser Fusing of Flame Sprayed Coatings," *Welding J.,* 1978, December, pp. 29-32.
4. K.L. Wang, Y.M. Zhu, and W.M. Steen: "Laser Remelting of Plasma Sprayed Coatings," *J. Laser Appl.,* 2000, *12*(4), pp. 175-78.
5. X.C. Yang, Y.H. Han, X.K. Wang, and H.W. Gu: "Microstructure and Performance of Laser Cladding NiCrBSi Alloy," in *Applications of Lasers and Electro-Optics, Proceedings of ICALEO 87,* San Diego, CA, 1987, Laser Institute of America, Orlando, FL, pp. 209-20.
6. Y. Longa and M. Takemoto: "Laser Processing of High-Chromium Nickel-Chromium Coatings Deposited by Various Thermal Spraying Methods," *Corrosion,* 1994, *50*(11), pp. 827-37.

7. Y. Longa and M. Takemoto: "High-temperature Corrosion of Laser-Glazed Alloys in Na_2SO_4-V_2O_5," *Corrosion,* 1992, *48*(7), pp. 599-607.
8. T.A. Mahank, J. Singh, and A.K. Kulkarni: "Laser Glazing of Plasma Sprayed Ni-Cr-Al-Y Alloy," *Mater. Manuf. Process.,* 1998, *13*(6), pp. 829-39.
9. A.H. Dent, A.J. Horlock, D.G. McCartney, and S.J. Harris: "The Corrosion Behavior and Microstructure of High-Velocity Oxy-Fuel Sprayed Nickel-Base Amorphous/Nanocrystalline Coatings," *J. Thermal Spray Technol.,* 1999, *8*(3), pp. 399-404.
10. H. Edris, D.G. McCartney, and A.J. Sturgeon: "Microstructural Characterization of High-Velocity Oxy-Fuel Sprayed Coatings of Inconel 625," *J. Mater. Sci.* 1997, *32,* pp. 863-72.
11. S. Tobe, Y. Andoh, K. Hidaka, K. Tanaka, S. Nishimura, K. Kawaharada and K. Shirai: "High Temperature Corrosion Resistance of Newly Developed Cr-Based Alloy Coatings," *Proceedings of UTSC'99,* E. Lugsheider and P.A. Kammer, ed., ASM Thermal Spray Society, DVS German Welding Society, Düsseldorf, Germany, 1999, pp. 296-300.
12. *ASM Metals Handbook—Properties and Selection: Stainless Steels, Tool Materials and Special-Purpose Metals,* 9th ed., Vol. 3, ASM, Metals Park, OH, USA, 1980, p. 145.